Effect of aluminium dust on secondary organic aerosol formation in m-xylene/NO

ARTICLE *in* SCIENCE CHINA EARTH SCIENCE · FEBRUARY 2015

Impact Factor: 1.49 · DOI: 10.1007/s11430-014-5023-0

8 AUTHORS, INCLUDING:

Qingxin Ma

Chinese Academy of Sciences

31 PUBLICATIONS **286** CITATIONS

SEE PROFILE

Biwu Chu

Chinese Academy of Sciences

15 PUBLICATIONS **59** CITATIONS

SEE PROFILE

Yongchun Liu

Chinese Academy of Sciences

53 PUBLICATIONS **522** CITATIONS

SEE PROFILE

Junhua Li

Tsinghua University

192 PUBLICATIONS **3,340** CITATIONS

SEE PROFILE

SCIENCE CHINA
Earth Sciences

• RESEARCH PAPER •

February 2015 Vol.58 No.2: 245–254
doi: 10.1007/s11430-014-5023-0

Effect of aluminium dust on secondary organic aerosol formation in *m*-xylene/NO_x photo-oxidation

LIU Chang[1], MA QingXin[2], CHU BiWu[2], LIU YongChun[2], HE Hong[2], ZHANG XiaoYe[1*], LI JunHua[3] & HAO JiMing[3]

[1] *Chinese Academy of Meteorological Sciences, Beijing 100081, China;*
[2] *Research Center for Eco-Environmental Sciences, Chinese Academy of Sciences, Beijing 100085, China;*
[3] *School of Environment, Tsinghua University, Beijing 100084, China*

Received May 15, 2014; accepted August 26, 2014; published online December 18, 2014

As an important anthropogenic volatile organic compound (VOC), *m*-xylene has attracted numerous attentions due to its potential in secondary organic aerosol (SOA) formation. In this study, effects of aluminium dust seeds (boehmite and alumina) on SOA yield and aerosol size in *m*-xylene/NO_x photo-oxidation were investigated in a 2 m^3 smog chamber at 30°C and 50% relative humidity. Compared to the seed-free system, the presence of aluminium seeds resulted in an increase in the SOA yield, and also enhanced the O_3 concentration in the chamber. The photolysis of O_3 is a major source of OH radical, which is the most important oxidant of *m*-xylene. The increase in O_3 concentration could result in the generation of more OH radicals, and finally contribute to the SOA formation. Seed particles influence the SOA size mainly by acting as condensation nuclei. Semi-volatile organic compounds (SVOCs) were condensed onto these nuclei, resulting in the increase in SOA size. However, when aluminium seeds with high concentrations were introduced into the system, SVOCs that had been condensed onto each particle were dispersed by these seeds, leading to the reduction in aerosol size.

aromatic hydrocarbon, *m*-xylene, aluminium, SOA, aerosol size, smog chamber

Citation: Liu C, Ma Q X, Chu B W, et al. 2015. Effect of aluminium dust on secondary organic aerosol formation in *m*-xylene/NO_x photo-oxidation. Science China: Earth Sciences, 58: 245−254, doi: 10.1007/s11430-014-5023-0

Aromatic hydrocarbons such as benzene, toluene, and *m*-, *p*-, *o*-xylene are important constituents of urban atmosphere, accounting for 20%–30% of total volatile organic compounds (VOCs) (Calvert et al., 2002). Outdoor aromatics are mainly from vehicle exhaust, gasoline evaporation, bio-decomposition of wastes, and solvent usage, whereas indoor aromatics originate mainly from adhesives and tobacco smoke (Na et al., 2005; Zhang Y et al., 2013). Aromatic hydrocarbons are proved to have a negative effect on human health (Guo et al., 2004). Meanwhile, the atmospheric transformation of aromatic species has attracted numerous attentions due to their potential in ozone production and secondary organic aerosol (SOA) formation (Loza et al., 2012; White et al., 2014). For example, field measurements carried out in Seoul, Korea, proved that xylene is the largest contributor to local ozone formation (Na et al., 2005). SOA tracer-based measurement studies indicated that toluene and xylene contribute more to SOA formation than biogenic VOCs (isoprene and monoterpenes) in Guangzhou (Wang et al., 2013).

The atmospheric photo-oxidation of aromatics yields semi-volatile (or nonvolatile) species, which then partition between the gas and particulate phases, resulting in the formation of SOA (Hallquist et al., 2009; Kroll and Seinfeld, 2008). A gas-aerosol absorptive partitioning model of or-

*Corresponding author (email: xiaoye@cams.cma.gov.cn)

ganic aerosol was developed by Pankow (1994a, 1994b), and was further extended to SOA formation by Odum et al. (1996). SOA yield Y (defined as $\Delta M/\Delta HC$, the amount of aerosol formed per hydrocarbon reacted) is commonly used to represent the SOA formation potential of the hydrocarbons (Pandis et al., 1992), and has been proved to depend largely on the total mass concentration of the generated organic aerosol (M_o, μg m^{-3}) (Odum et al., 1996, 1997):

$$Y = \frac{\Delta M}{\Delta HC} = M_o \sum_i \frac{\alpha_i K_{om,i}}{1 + K_{om,i} M_o}, \quad (1)$$

where i represents the serial number of the produced semi-volatile species, ΔHC (μg m^{-3}) is the reacted hydrocarbon concentration, α_i and $K_{om,i}$ (m^3 μg^{-1}) are the mass-based stoichiometric coefficient and the gas-particle partition constant for product i, respectively. M_o directly affects the gas-particles partition by acting as the medium into which oxidation species can be absorbed. Therefore, products with relatively high vapor pressure may be absorbed into the particulate phase even though the products are present at concentrations below their saturation point.

The generation of semi-volatile compounds (SVOCs) and nonvolatile products as well as the following partitioning process depends on a variety of ambient conditions, such as temperature, relative humidity (RH), the mixing ratio of NO_x and hydrocarbon, and ultraviolet (UV) intensity (Hallquist et al., 2009; Jia and Xu, 2014). These factors potentially influence both the chemical mechanisms and the phase partitioning thermodynamics (Hallquist et al., 2009). For example, Takekawa et al. (2003) found that under the condition of the same SOA concentration, the SOA yield at 283 K was approximately twice that at 303 K. Song et al. (2005) demonstrated that larger hydrocarbon to NO_x ratio leads to higher SOA formation potential in *m*-xylene/NO_x photoreaction system. Zhou et al. (2011) found that high relative humidity promoted the SOA formation in the photo-oxidation of xylenes and toluene. The humidity could influence the content of particle water, and the SOA yield was positively correlated with the particle water content (Zhou et al., 2011). Previous researches also proved that inorganic seeds, especially acidic particles such as ammonium sulfate, play a critical role in SOA formation (Cao and Jang, 2010).

New particles formation is usually accompanied by the growth in aerosol size and the change in size distribution (Liu et al., 2013a; Warren and Seinfeld, 1985). As a significant characteristic of aerosols, particle size greatly influences the cloud condensation nuclei (CCN) activity, light scattering property, and lifetime of aerosols. Therefore, research on the variation of aerosol size during SOA formation is of great significance. During homogeneous nucleation process, the partitioning of generated semi-volatile and nonvolatile species to particulate phase results in the generation of SOA particles, and the coagulation of these species leads to the further growth in aerosol size (Hallquist et al., 2009). If pre-existing particles (i.e., seeds) coexist with the formed SVOC species, the products preferred to condense and coagulate to the seed surfaces to form SOA particles. This heterogeneous nucleation process also leads to the change in aerosol size (Ma et al., 2012). Although the change of aerosol size during SOA formation has been observed in previous research, the factors that influence the size still need further study.

In this work, formation of SOA particles and change of aerosol size during *m*-xylene/NO_x photo-oxidation was studied in an indoor smog chamber. Aluminium dust including boehmite (AlOOH) and alumina (Al_2O_3) were chosen as seed particles. Boehmite is a major component of aluminium ore bauxite (Mameli et al., 2007), and alumina is usually chosen as the model oxide for mineral dust in laboratory researches (Liu et al., 2012; Ma et al., 2008; Tong et al., 2010). The influences of aluminium seeds on SOA yield and SOA size were also discussed.

1 Experimental section

1.1 Chamber facility

All experiments were carried out in an indoor smog chamber, which was described in detail previously (Chu et al., 2012; Liu et al., 2013a; Zhao et al., 2008). Briefly, a cuboid reactor, with a volume of 2 m^3 and a surface-to-volume ratio of 5 m^{-1}, was constructed from 50 μm-thick FEP-Teflon film (Toray Industries, Inc., Japan). The chamber was located in a temperature controlled room (Escpec SEWT-Z-120). During the experiments, the chamber was irradiated by 40 black lights (GE F40T12/BLB, 40 W, peak intensity at 365 nm). UV radiation (measured by Handy UV-A), temperature, and relative humidity (measured by Vaisala HMT 333) were monitored continuously.

Boehmite and alumina seeds were on-line produced by a spray pyrolysis setup, which was also described previously (Liu et al., 2010, 2013b). Boehmite seed aerosols were generated by atomizing alumisol (AlOOH, Lot No. 2205, Kawaken Fine Chemicals Co., Ltd.). The concentration of the alumisol precursor was 1.0 wt% calculated according to Al_2O_3 content. The flow rate of carrier air was kept at 2.0 L min^{-1}. The generated aerosol seeds were dried by a diffusion dryer and then introduced into the chamber through a neutralizer (TSI Model 3077). Alumina seeds were generated by carrying the atomized alumisol particles through a tubular furnace (maintained at 1000°C) and introduced them into the chamber. The concentration of seeds was adjusted by changing the atomizing time, and was monitored using a scanning mobility particle sizer (SMPS, TSI 3936), which consists of a nano differential mobility analyzer (DMA, TSI 3085) and a condensation particles counter (CPC, TSI 3025A). The particle size distributions of produced seeds are illustrated in Figure 1, and the concentration and diame-

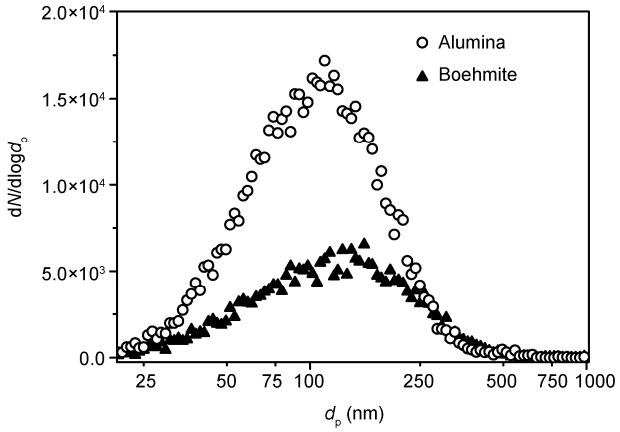

Figure 1 Particle size distributions of 14.81 μg m^{-3} boehmite seeds and 20.47 μg m^{-3} alumina seeds.

ter of seeds in each experiment are listed in Table 1. The obtained boehmite and alumina seed particles were spherical-shaped as shown by electron microscopy measurements (Liu et al., 2010, 2013b).

After the introduction of seed particles, *m*-xylene (Analytical reagent, Sigma Aldrich Fluka) was injected by syringe into a heated furnace (maintained at 160°C) and then carried into the chamber by 5 L min^{-1} purified air. A gas chromatograph (GC, Beifen SP-3420) equipped with a DM-5 column (30 m × 0.53 mm × 1.5 μm, Dikma) and flame ionization detector (FID) measured the concentration of *m*-xylene every 15 min. NO_x (NO and NO_2) were carried into the chamber by purified dry air. NO_x and O_3 (generated during photo-oxidation) were detected by a NO_x analyzer (Thermo Environmental Instruments, Model 42C) and an O_3 analyzer (Thermo Environmental Instruments, Model 49C), respectively. In all experiments, the aerosol mass concentrations were determined from the observed total aerosol volume assuming the particles were geometrically spherical with a density of 1.0 g cm^{-3}. Count median diameter determined by SMPS was used to express the particle size of aerosols.

1.2 Experimental conditions

By using the smog chamber, a series of experiments were carried out for *m*-xylene/NO_x photo-oxidation. Before each experiment, the chamber was flushed continuously by purified dry air for 40 h, including exposure to UV irradiation for 20 h. Finally, humid air was introduced into the chamber to obtain a specific RH of 50%. When temperature and humidity were stabilized at around 30°C and 50% RH, respectively, aluminium seeds, *m*-xylene, NO, and NO_2 were injected successively into the chamber. The photochemical reaction was then conducted for 6 h with the black lights on. Experimental conditions and results are listed in Table 1. The "Experiment No." was designed to [*m*-xylene concentration] HC-[seeds concentration][seeds name]. "Alu" and "Boe" were referred to alumina seeds and boehmite seeds,

Table 1 Experimental conditions and results of *m*-xylene/NO_x photo-oxidation[a)]

Experiment No.	HC_0 (ppm)	$Seed_0$ (μg m^{-3})	$Seed_0$ (×10^3 cm^{-3})	$NO_{x,0}$ (ppb)	$NO_{2,0}$ (ppb)	$HC_0/NO_{x,0}$	d_{seed} (nm)	d_{SOA} (nm)	T_{Mo} (h)	ΔM_o (μg m^{-3})	ΔHC (ppm)	Y (%)
1.1HC-0	1.10	0	0	62.9	62.9	8.7	0	222	1.9	12.5830	0.2459	1.205
2.1HC-0	2.11	0	0	120.8	117.7	8.8	0	297	1.6	56.1149	0.4703	2.794
3.2HC-0	3.21	0	0	197.8	179.8	8.5	0	331	1.2	48.9764	0.5455	2.102
4.2HC-0	4.23	0	0	241.8	244.2	8.7	0	301	1.1	44.5099	0.5346	1.950
1.1HC-7Alu	1.15	7.22	3.31	64.1	63.0	9.0	105	252	1.9	14.8694	0.2733	1.274
1.1HC-20Alu	1.17	20.47	9.74	64.2	63.4	9.1	103	185	1.9	22.3070	0.2700	1.935
1.1HC-35Alu	1.04	35.05	15.5	64.9	61.6	8.2	107	173	2.0	19.5561	0.2707	1.692
2.1HC-8Alu	2.26	8.06	3.50	119.9	124.8	9.2	105	339	1.6	72.3456	0.5368	3.156
2.1HC-23Alu	2.26	22.75	8.99	122.1	116.7	9.4	108	267	1.5	63.3100	0.5000	2.940
2.1HC-36Alu	2.12	35.99	18.2	121.4	124.8	8.6	103	211	1.6	42.2300	0.4300	2.320
3.2HC-8Alu	3.19	8.63	5.06	183.9	174.1	8.9	96	356	1.2	49.5035	0.4358	2.660
3.2HC-38Alu	3.05	38.26	19.5	184.3	183.6	8.3	109	250	1.1	34.6021	0.4669	1.735
1.1HC-9Boe	1.16	9.12	3.98	65.3	60.9	9.2	118	221	2.0	22.3043	0.2895	1.804
1.1HC-52Boe	1.15	51.85	18.5	65.4	67.8	8.6	104	164	1.9	14.1466	0.2726	1.215
2.1HC-15Boe	2.15	14.81	4.00	117.6	121.3	9.0	120	315	1.7	62.9249	0.4754	3.100
2.1HC-35Boe	2.13	34.79	11.1	115.4	121.0	9.0	113	207	1.4	20.3924	0.3587	1.331
2.1HC-75Boe	2.27	74.84	19.2	115.9	120.3	9.6	117	199	1.7	51.5122	0.4727	2.552
3.2HC-11Boe	3.13	11.43	5.26	178.3	191.1	8.5	101	368	1.2	37.9600	0.4975	1.787
3.2HC-68Boe	3.19	67.97	18.2	183.1	182.3	8.7	114	259	1.2	40.1168	0.5720	1.642

a) HC_0, initial concentration of *m*-xylene; $seed_0$, initial concentration of alumina or boehmite seeds; $NO_{x,0}$, initial concentration of NO; $NO_{2,0}$, initial concentration of NO_2; $HC_0/NO_{x,0}$ (ppb/ppb), initial molar ratio of *m*-xylene to NO_x ($NO+NO_2$); d_{seed}, main diameter of seeds; d_{SOA}, final diameter of SOA aerosol; T_{Mo}, time to determine the SOA yield; ΔM_o, mass concentration of generated SOA; ΔHC, total concentration of consumed *m*-xylene; Y, overall aerosol yield. All of the experiments were carried out at 30°C and 50% RH with UV irradiation.

respectively. For example, "1.1HC-7Alu" represents the experiment with 1.1 ppm *m*-xylene and 7 μg m^{-3} alumina seeds. The initial *m*-xylene concentration levels were kept at 1.1, 2.1, or 3.2 ppm. All experiments were conducted at a temperature of 30±0.5°C and 50% RH with UV irradiation.

1.3 Calculation of SOA yield

Due to the deposition of particles onto the chamber wall, the measured aerosol concentration in each experiment has to be corrected. The particle deposition rate is proportional to the number concentration of aerosols N (particles cm^{-3}) and depends on particle size d_p (nm), leading to first-order kinetics (Bowman et al., 1997; Carter et al., 2005):

$$\frac{dN(d_p,t)}{dt} = -k_{dep}(d_p)\cdot N(d_p,t), \quad (2)$$

where k_{dep} (h^{-1}) is the deposition rate constant. The value of k_{dep} depended on d_p, and can be expressed as follows (Chu et al., 2012; Takekawa et al., 2003):

$$k_{dep}(d_p) = a\times d_p^{\ b} + c/d_p^{\ d}. \quad (3)$$

In this work, the optimized values of a–d were 6.4579×10^{-7}, 1.7841, 13.1947, and −0.9566, respectively (Chu et al., 2012; Liu et al., 2013a).

Hydrocarbons were consumed by deposition on the walls as well as by photo-oxidation. The deposition rate of *m*-xylene was 0.6% h^{-1}, based on observation of hydrocarbon decay under dark conditions. Concentrations of reacted hydrocarbons were calculated from the consumed and deposited concentrations.

SOA yields were calculated according to eq. (1). To reduce error due to the correction of wall losses, concentrations of the generated aerosol ΔM_o and the reacted *m*-xylene ΔHC were determined at a correction time T_{Mo} (h), as described in a previous research (Chu et al., 2012):

$$T_{Mo} = T_{Mo,\text{ seed-free}} \times \frac{T_{\max(NO_x),\text{ seeded}}}{T_{\max(NO_x),\text{ seed-free}}}, \quad (4)$$

where $T_{Mo,\text{ seed-free}}$ refers to the time when the measured particle concentration reached its maximum in the seed-free experiments. $T_{\max(NO_x),\text{ seeded}}$ and $T_{\max(NO_x),\text{ seed-free}}$ are the time when NO_x concentration reached its maximum in the seeded and seed-free experiments, respectively.

2 Results and discussion

2.1 Generation of SOA aerosols

A series of *m*-xylene/NO_x photo-oxidation experiments with alumina or boehmite seeds were performed in smog chamber at 30°C and 50% RH. The experimental results are listed in Table 1. Figure 2 shows typical time variations of

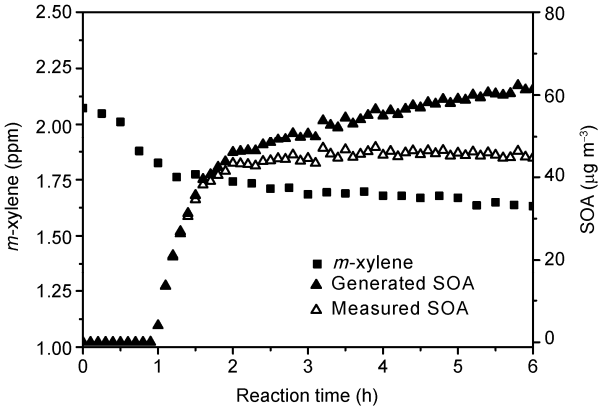

Figure 2 Typical time variations of *m*-xylene and SOA concentrations observed from *m*-xylene/NO_x photo-oxidation (Experiment No. 2.1HC-0).

m-xylene and SOA concentrations observed in 2.1 ppm *m*-xylene photo-oxidation (2.1HC-0). Generated SOA contains both measured SOA and the deposited SOA corrected for wall losses. As seen from Figure 2, the consumption of *m*-xylene was detected at the beginning of irradiation. Generation of semi-volatile or nonvolatile species, such as benzaldehyde, methylphenol, glyoxal, and methylfuran (Calvert et al., 2002), dominated the first hour of irradiation, and then formation of SOA particles became obvious. After about 2 h irradiation, the concentration of measured SOA maintained steady. However, the concentration of generated SOA continued to increase.

Formation of SOA particles in *m*-xylene photo-oxidation with or without alumina seeds was compared and is shown in Figure 3. Alumina seeds appeared to have an important influence on SOA generation. Compared to the seed-free experiments, SOA formation in experiments with alumina seeds was obviously promoted, especially in experiments with 1.1 ppm (Figure 3(a)) or 2.1 ppm (Figure 3(b)) *m*-xylene. The enhancement on SOA generation was much greater in experiments with fewer alumina seeds. For example, the promotion effect of experiment with 7.22 μg m^{-3} alumina seeds (line 1.1HC-7Alu in Figure 3(a)) was greater than that with 35.05 μg m^{-3} alumina (line 1.1HC-35Alu in Figure 3(a)). Similar effect was also observed when boehmite seeds presented in the experiments (data not show here). It is implied that aluminium seeds could promote the generation of SOA particles, and might have influence on the SOA yield. This promotion effect was less significant for experiments with high concentration *m*-xylene (Figure 3(c)). We consider that when high concentration of *m*-xylene was introduced into the chamber, the formation of semi-volatile and nonvolatile species was greatly enhanced, and the influence of alumina seeds on their concentrations was not so significant.

2.2 Effect of seeds on SOA yield

A gas-aerosol absorptive partitioning model developed by

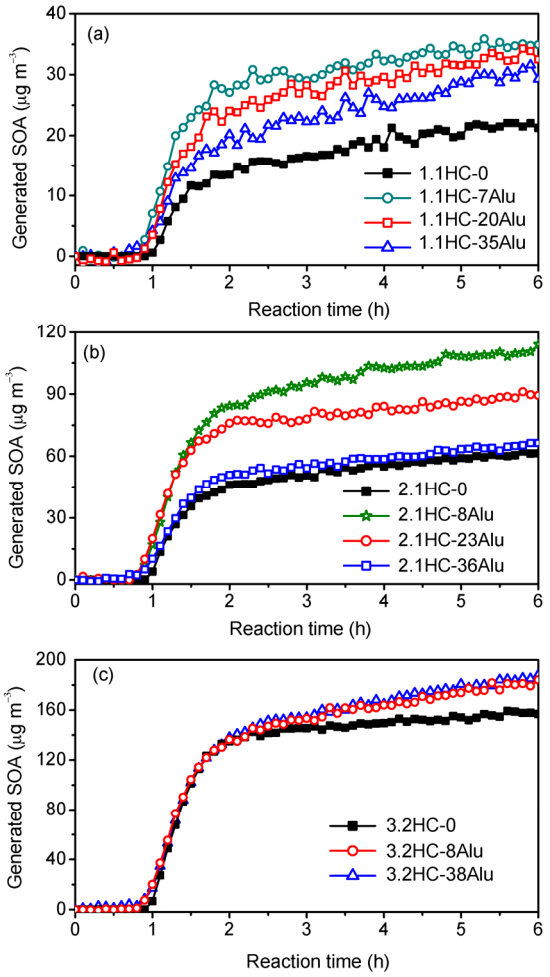

Figure 3 Mass concentrations of generated SOA observed from (a) 1.1, (b) 2.1, and (c) 3.2 ppm *m*-xylene photo-oxidation systems with different concentrations of alumina seeds at 30°C and 50% RH.

Pankow (1994a, 1994b) and Odum et al. (1996) is widely used to describe SOA formation. In this model, SOA yield Y is proved to depend strongly on the total mass concentration of the organic aerosol M_o (as described by eq. (2)). One or two-product models (i=1 or 2 in eq. (2)) are typically employed to obtain the yield curve. Previous studies suggested that the two-product model is needed to fit the experimental data (Odum et al., 1996, 1997). However, Takekawa et al. (2003) observed that a one-product model reproduced correctly the experimental results. Henry et al. (2008) compared the yield curves fitted by one-product and two-product model, and proposed that one-product model is suitable to describe the relationship between aerosol yield Y and aerosol mass M_o.

Experimental data in this work were also analyzed according to the gas-aerosol absorptive partitioning model. Figure 4 shows yield curves fitted via both one-product model (solid line) and two-product model (dotted line). The parameters α and K determined from the fitting were listed in Table 2. Figure 4 clearly showed that the fitting results obtained from one- or two-product model were quite similar for both seed-free and seeded experiments. Besides, the coefficients of determination of one-product fit (R^2>0.89) are even better than the coefficients of two-product fit (R^2>0.84). Therefore, we consider one-product model is suitable to describe the relationship between the yield and the generated aerosol mass for *m*-xylene system.

SOA yield curves of *m*-xylene seed-free and seeded experiments obtained from one-product partitioning model were compared and are shown in Figure 5. Curves of seeded

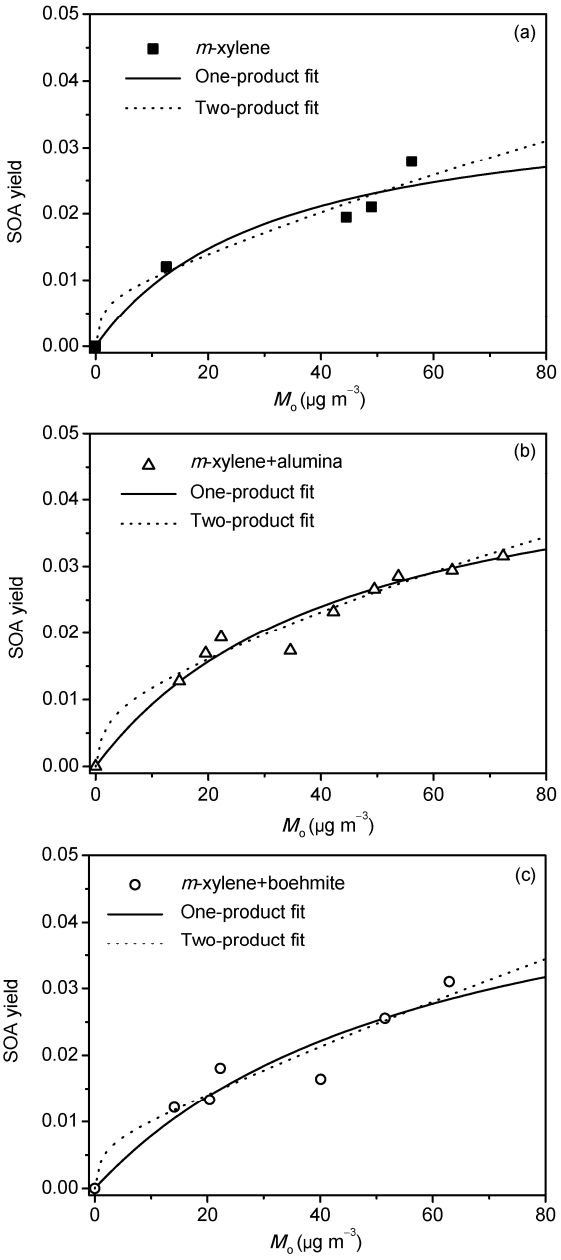

Figure 4 SOA yield (Y) as a function of generated organic aerosol mass (M_o) for (a) *m*-xylene photo-oxidation, and *m*-xylene photo-oxidation with (b) alumina seeds or (c) boehmite seeds. The solid and dotted lines represent the fit of one-product and two-product model to the data. All experiments were carried out at 30°C and 50% RH.

Table 2 Parameters determined from the fit of one-product model and two-product model [a)]

Experiments	One-product model			Two-product model				
	α	K	R^2	α_1	K_1	α_2	K_2	R^2
m-xylene	0.03752	0.03232	0.922	0.00741	1 [b)]	0.13803	0.00259	0.842
m-xylene+alumina	0.05078	0.02237	0.952	0.00879	0.66254	0.10687	0.00398	0.947
m-xylene+boehmite	0.05597	0.01634	0.894	0.0072	1 [b)]	0.61507	0.00059	0.873

a) α, Mass-based stoichiometric coefficient; K, gas-particle partition constant; R^2, coefficient of determination. b) Upper limit value set.

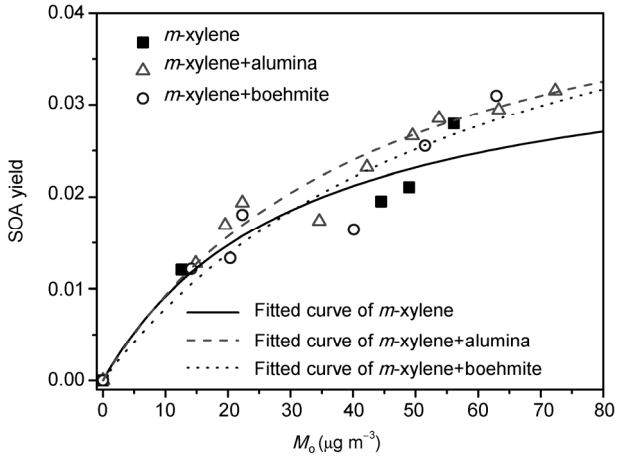

Figure 5 Comparison of yield curves of *m*-xylene, *m*-xylene + alumina, and *m*-xylene + boehmite photo-oxidation system. All experiments were carried out at 30°C and 50% RH. Yield curves were obtained by fitting data according to one-product model.

experiments, especially with the alumina seeds, are higher than the curve of seed-free experiments. This implies that both alumina and boehmite have promotion effect on SOA formation in *m*-xylene photo-oxidation experiments. These results also conform to the generated SOA concentration results (as illustrated in Figure 3).

Aerosol yields from the photo-oxidation of aromatic hydrocarbons have been shown to be highly sensitive to the NO_x level (Hurley et al., 2001; Song et al., 2005). This dependence of SOA formation on the NO_x level has been proposed to be the result of differences in the concentrations of various oxidants, such as OH, O_3, and NO_3 (Hurley et al., 2001). These oxidants are formed during the photo reaction of NO_x. They initiate the degradation of VOCs, determine the distribution and volatility of products, and therefore are considered as the controlling factors in SOA formation. As one major oxidant in nighttime troposphere, NO_3 radical decomposes quickly under illumination. Accordingly, the role of NO_3 radicals in the formation of *m*-xylene SOA in this work is negligible. The reaction of aromatic hydrocarbons with OH radicals represents the major atmospheric loss process during daylight hours (Smith et al., 1999). OH radicals can react with aromatic compounds by abstracting hydrogen atoms from the alkyl group or by adding to the aromatic ring (Smith et al., 1999). Due to the limitation of instruments, however, the OH radicals were not monitored in our chamber. Although O_3 is less reactive than OH radicals, O_3 contributes to the SOA formation because that the photolysis of O_3 is a major source of OH production (Wine and Nicovich, 2012):

$$O_3 \xrightarrow[h\nu]{300\ \text{nm}<\lambda<340\ \text{nm}} O_2 + O(^1D) \quad (5)$$

$$O(^1D) + H_2O \longrightarrow 2OH \quad (6)$$

The concentrations of O_3 were on-line detected in our work. *m*-xylene/NO_x photo-oxidation systems with different concentrations of alumina seeds were taken as the examples to show the dynamic change of O_3 concentration during the photo reaction (Figure 6). O_3 concentrations in alumina seeded experiments were much higher than the concentrations in seed-free experiments. Thus, the increase in O_3 concentration will result in the production of more OH radicals, and finally contributes to the SOA formation.

Previous researches proved that the concentration of O_3 during photochemical smog is controlled by the following reactions:

$$NO_2 \xrightarrow[h\nu]{\lambda<430\,\text{nm}} O(^3P) + NO \quad (7)$$

$$O(^3P) + O_2 \rightarrow O_3 \quad (8)$$

$$O_3 + NO \rightarrow O_2 + NO_2 \quad (9)$$

$$O_3 + NO_2 \rightarrow O_2 + NO_3 \quad (10)$$

$$O_3 + \text{hydrocarbon} \rightarrow \text{ozonide} \rightarrow \text{products} \quad (11)$$

Therefore, factors affecting the concentrations of NO, NO_2, or hydrocarbon species might influence the O_3 concentration. Aluminium dust is very reactive to NO and NO_2, meanwhile the adsorption of hydrocarbon compounds could happen on aluminium dust surface (Usher et al., 2003). Accordingly, the reaction of alumina seeds with NO, NO_2, and hydrocarbon species might contribute to the change of O_3 concentration. The promotion effect of aluminium seeds on O_3 concentration shown in Figure 6 was consistent with the increase in SOA concentration (Figure 3), indicating that enhancement on O_3 concentration contributed to SOA formation.

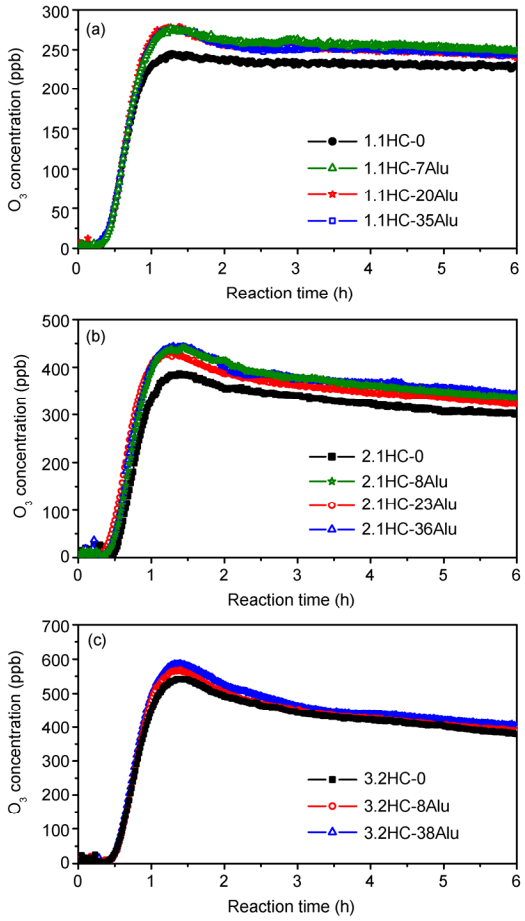

Figure 6 Dynamic change of O_3 concentration in (a) 1.1, (b) 2.1, and (c) 3.2 ppm *m*-xylene/NO_x photo-oxidation systems with different concentrations of alumina seeds at 30°C and 50% RH.

2.3 Effect of seeds on number concentration and aerosol size

New aerosol formation is always accompanied by increase in number concentration and change in size distribution. The influence of aluminium seeds on the number concentration and aerosol size was investigated in this work. The 2.1 ppm *m*-xylene photo-oxidation system was taken as an example to show the change in particle size caused by aluminium seeds. As shown in Figure 7(a), there was no new aerosol formation at the beginning of seed-free *m*-xylene photo-oxidation. The first 1 h irradiation was dominated by the generation of free radicals (such as OH and NO_3) and O_3 via the photo reaction, meanwhile, SVOCs formed via the oxidation of *m*-xylene accumulated at this stage. After 1 h, the number concentration and particle size of aerosols increased rapidly, indicating numerous new aerosol particles generated through a homogeneous nucleation process. The drastic generation of aerosols lasted nearly 1 h. After 2 h irradiation, the total number and mass concentrations of aerosols were 5.68×10^3 particles cm^{-3} and 62.8 μg m^{-3}, respectively. The mean diameter was 262 nm. After that, the

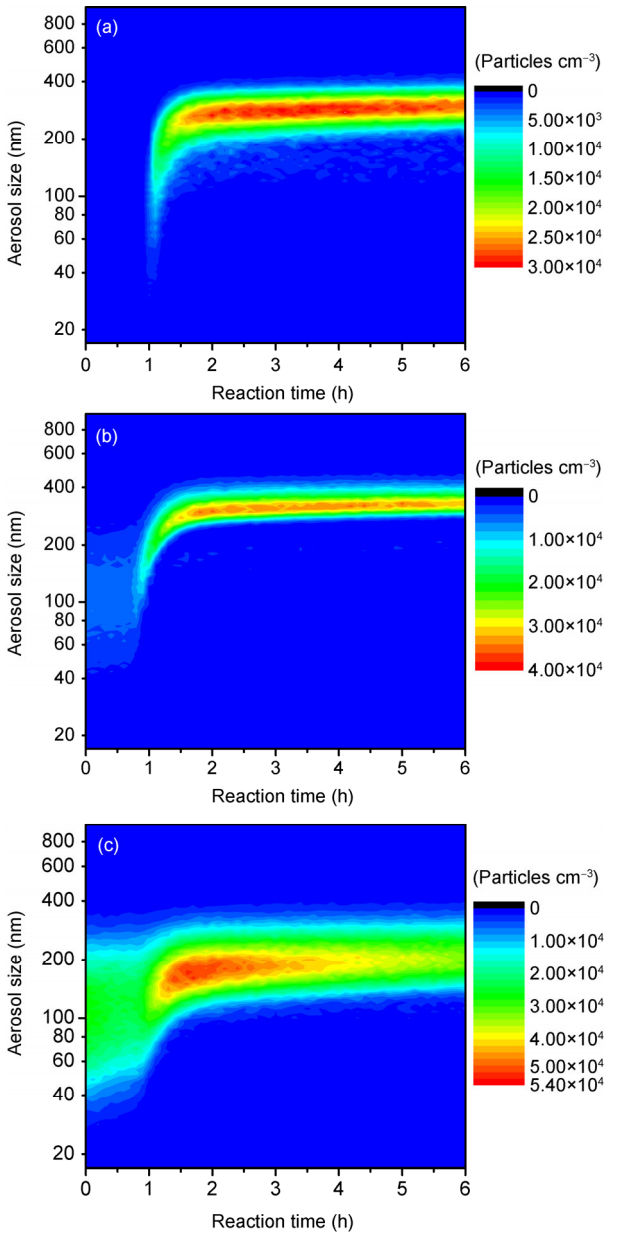

Figure 7 Change of aerosol size distribution and number concentration as a function of time in experiments of (a) 2.1HC-0, (b) 2.1HC-8Alu, and (c) 2.1HC-36Alu.

generation of aerosols slowed down and the final concentration of aerosols was 71.5 μg m^{-3} at the end of reaction. Meanwhile, the increase in particle size (to 297 nm at the end of reaction) as well as the decrease in total number concentration (to 4.63×10^3 particles cm^{-3}) indicated the coagulation among particles dominated the last 4 h irradiation.

Unlike the seed-free experiment, formation of new aerosols during seeded experiments was via a heterogeneous nucleation process. When 8.06 μg m^{-3} (3.5×10^3 particles cm^{-3}) alumina was injected into the smog chamber (Figure 7(b)), these alumina seeds acted as nuclei and the formed

SVOC species preferred to condense and coagulate onto the seed surfaces to generate SOA particles. Compared to the seed-free experiment, the new particle formation in this seeded experiment was about 10 min earlier because of the pre-existing condensation nuclei. The concentration of aerosols increased to 86 μg m^{-3} (4.65×10^3 particles cm^{-3}) after 2 h irradiation, meanwhile the size grew from 122 to 309 nm. The mass concentration increased slightly to 86.8 μg m^{-3} at the end of reaction. The coagulation also resulted in the reduction in number concentration (to 3.73×10^3 particles cm^{-3} at the end of reaction) and increase in particle size (to 339 nm).

When alumina seeds with higher concentration (35.99 μg m^{-3}, Figure 7(c)) were injected into the chamber, rapid generation of aerosol particles was also started at about 1 h irradiation. After 2 h reaction, the mass concentration of total aerosols increased to 77 μg m^{-3}, and the aerosol size increased to 183 nm. After that, although a slight growth of aerosol particles (211 nm at the end of reaction) was detected, the decrease in both number and mass concentration indicated that high seeds loading resulted in more aggravate deposition.

The final aerosol size was various in above reactions, and was in close relation with the concentration of seeds. The final aerosol size of 2.1 ppm *m*-xylene seed-free experiment was 297 nm. When 8.06 μg m^{-3} alumina was added into the reaction, the final size increased to 339 nm. When the seeds concentration increased to 35.99 μg m^{-3}, however, the aerosol diameter was only 211 nm, much smaller than the final size obtained in seed-free experiment.

To investigate the effect of seeds concentration on aerosol size, we compared the final diameter of aerosols formed in both alumina seeded and boehmite seeded systems. As illustrated by Figure 8, all the aerosol diameters obtained with low seeds concentration (about 10 μg m^{-3}) were larger than those measured in the seed-free experiments. Nevertheless with high seeds concentration, the final size decreased significantly with increasing seeds concentration. For instance, in the 3.2 ppm *m*-xylene photo-oxidation, aerosol size increased from 331 to 368 nm because of the injection of 11.43 μg m^{-3} boehmite seeds, but reduced to 259 nm when the seeds concentration increased to 67.97 μg m^{-3}.

This variation of aerosol size is similar with our previous research on α-pinene/NO_x photo-oxidation (Liu et al., 2013a). In that study, aerosol size obtained in experiments with a low concentration of seeds was larger than the size measured in seed-free experiment. We proposed that the increase in aerosol size was due to the coagulation and condensation of SVOC species onto the existing seed surface during the SOA formation (Liu et al., 2013a). However, when seed concentration exceeded about 5 μg m^{-3}, the final size of aerosol decreased obviously with the increase in seed concentration. SVOCs were dispersed by these seeds,

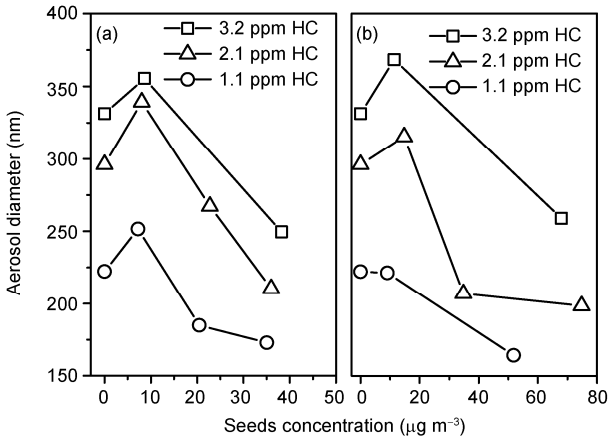

Figure 8 Change of aerosol size as a function of (a) alumina and (b) boehmite seeds concentration. Aerosol size is described by the final value of count median diameter obtained in *m*-xylene photo-oxidation systems at 30°C and 50% RH with the reaction time of 6 h. Each data point corresponds to a separate experiment.

and the amount of SVOCs that was condensed onto each particle was reduced greatly, leading to the reduction in aerosol size. Seed effect on aerosol final size has been observed in *m*-xylene/NO_x system with boehmite or alumina seeds, and α-pinene/NO_x system with alumina seeds. The similar results imply that seed particles influence the SOA size mainly by acting as condensation nuclei. This seed effect on aerosol size might also be applicable to other kinds of seeds. However, it still needs further investigation.

2.4 Atmospheric implications

Traffic exhaust is a significant source of *m*-xylene (Garcia et al., 2014; Liandi et al., 2001; Zhang Y et al., 2012). During the rush hour, the exhausted *m*-xylene greatly contributes to the SOA formation. Road traffic activities also lead to serious dust pollution (Almeida et al., 2006; Zhang et al., 2004; Huang et al., 2014). These dust particles are mainly eroded soils, and accordingly mineral particles are the primary constituents of dust (Zhang X Y et al., 2012, 2013). As the second largest components of mineral dust, aluminium particles could promote the formation of SOA from *m*-xylene/NO_x photo-oxidation process. This promotion effect will influence the contribution of *m*-xylene to regional SOA concentration, and also cause severe environmental problem such as haze. In addition, the size of aerosol particles formed during *m*-xylene/NO_x photo-oxidation could be influenced by aluminium particles. More aerosol particles with smaller size generate when aluminium particles with high concentration coexist with *m*-xylene, and consequently result in more serious risks to human health. Besides, the change of light scattering property due to the variation of particle size will also result in more complexity to the study on the environmental and climate effect of SOA particles.

3 Conclusion

Compared to the seed-free experiments, the SOA yields in *m*-xylene systems were promoted by the presence of aluminium seeds. O_3 concentrations in seeded experiments were much higher than the concentrations in seed-free experiments. The increase in O_3 concentration could result in more OH radical generation, and finally contributes to the SOA formation. Aluminium dust seeds also influenced the size of aerosol by acting as condensation nuclei. At low seed concentrations, SVOCs were condensed onto the pre-existing seed surfaces, leading to the growth in aerosol size. When aluminium seeds with higher concentrations were introduced into the smog chamber, the reduction in the SVOCs that condensed onto each seed particle resulted in the decrease in aerosol size.

This research was supported by the National Natural Science Foundation of China (Grant No. 41305116), the National Basic Research Program of China (Grant No. 2011CB403401), and the Specific Team Fund of Chinese Academy of Meteorological Sciences (Grant No. 2010Z002).

Almeida S M, Pio C A, Freitas M C, et al. 2006. Source apportionment of atmospheric urban aerosol based on weekdays/weekend variability: Evaluation of road re-suspended dust contribution. Atmos Environ, 40: 2058–2067

Bowman F M, Odum J R, Seinfeld J H, et al. 1997. Mathematical model for gas-particle partitioning of secondary organic aerosols. Atmos Environ, 31: 3921–3931

Calvert J G, Atkinson R, Becker K H, et al. 2002. The Mechanisms of Atmospheric Oxidation of Aromatic Hydrocarbons. New York: Oxford University Press. 540

Cao G, Jang M. 2010. An SOA model for toluene oxidation in the presence of inorganic aerosols. Environ Sci Technol, 44: 727–733

Carter W P L, Cocker D R, Fitz D R, et al. 2005. A new environmental chamber for evaluation of gas-phase chemical mechanisms and secondary aerosol formation. Atmos Environ, 39: 7768–7788

Chu B W, Hao J M, Takekawa H, et al. 2012. The remarkable effect of $FeSO_4$ seed aerosols on secondary organic aerosol formation from photooxidation of α-pinene/NO_x and toluene/NO_x. Atmos Environ, 55: 26–34

Garcia K O, Teixeira E C, Agudelo-Castañeda D M, et al. 2014. Assessment of nitro-polycyclic aromatic hydrocarbons in PM_1 near an area of heavy-duty traffic. Sci Total Environ, 479: 57–65

Guo H, Lee S C, Chan L, et al. 2004. Risk assessment of exposure to volatile organic compounds in different indoor environments. Environ Res, 94: 57–66

Hallquist M, Wenger J C, Baltensperger U, et al. 2009. The formation, properties and impact of secondary organic aerosol: Current and emerging issues. Atmos Chem Phys, 9: 5155–5236

Henry F, Coeur-Tourneur C, Ledoux F, et al. 2008. Secondary organic aerosol formation from the gas phase reaction of hydroxyl radicals with *m*-, *o*- and *p*-cresol. Atmos Environ, 42: 3035–3045

Huang X F, Yun H, Gong Z H, et al. 2014. Source apportionment and secondary organic aerosol estimation of $PM_{2.5}$ in an urban atmosphere in China. Sci China Earth Sci, 57: 1352–1362

Hurley M D, Sokolov O, Wallington T J, et al. 2001. Organic aerosol formation during the atmospheric degradation of toluene. Environ Sci Technol, 35: 1358–1366

Jia L, Xu Y. 2014. Effects of relative humidity on ozone and secondary organic aerosol formation from the photooxidation of benzene and ethylbenzene. Aerosol Sci Technol, 48: 1–12

Kroll J H, Seinfeld J H. 2008. Chemistry of secondary organic aerosol: Formation and evolution of low-volatility organics in the atmosphere. Atmos Environ, 42: 3593–3624

Liandi Z, Jie W, Haiyang Z, et al. 2001. Laser mass spectrometry for high sensitive and multi-component analysis of exhaust gas from vehicles. Chin Sci Bull, 46: 86–88

Liu C, Chu B W, Liu Y C, et al. 2013a. Effect of mineral dust on secondary organic aerosol yield and aerosol size in α-pinene/NO_x photo-oxidation. Atmos Environ, 77: 781–789

Liu C, Liu Y C, Ma Q X, et al. 2013b. Alumina with various pore structures prepared by spray pyrolysis of inorganic aluminum precursors. Ind Eng Chem Res, 52: 13377–13383

Liu C, Liu Y C, Ma Q X, et al. 2010. Mesoporous transition alumina with uniform pore structure synthesized by alumisol spray pyrolysis. Chem Eng J, 163: 133–142

Liu C, Ma Q X, Liu Y C, et al. 2012. Synergistic reaction between SO_2 and NO_2 on mineral oxides: A potential formation pathway of sulfate aerosol. Phys Chem Chem Phys, 14: 1668–1676

Loza C L, Chhabra P S, Yee L D, et al. 2012. Chemical aging of *m*-xylene secondary organic aerosol: Laboratory chamber study. Atmos Chem Phys, 12: 151–167

Ma J Z, Xu X B, Zhao C S, et al. 2012. A review of atmospheric chemistry research in China: Photochemical smog, haze pollution, and gas-aerosol interactions. Adv Atmos Sci, 29: 1006–1026

Ma Q X, Liu Y C, He H. 2008. Synergistic effect between NO_2 and SO_2 in their adsorption and reaction on γ-alumina. J Phys Chem A, 112: 6630–6635

Mameli P, Mongelli G, Oggiano G, et al. 2007. Geological, geochemical and mineralogical features of some bauxite deposits from Nurra (Western Sardinia, Italy): Insights on conditions of formation and parental affinity. Int J Earth Sci, 96: 887–902

Na K, Moon K-C, Kim Y P. 2005. Source contribution to aromatic VOC concentration and ozone formation potential in the atmosphere of Seoul. Atmos Environ, 39: 5517–5524

Odum J R, Hoffmann T, Bowman F, et al. 1996. Gas/particle partitioning and secondary organic aerosol yields. Environ Sci Technol, 30: 2580–2585

Odum J R, Jungkamp T P W, Griffin R J, et al. 1997. Aromatics, reformulated gasoline, and atmospheric organic aerosol formation. Environ Sci Technol, 31: 1890–1897

Pandis S N, Harley R A, Cass G R, et al. 1992. Secondary organic aerosol formation and transport. Atmos Environ, 26: 2269–2282

Pankow J F. 1994a. An absorption model of gas/particle partitioning of organic compounds in the atmosphere. Atmos Environ, 28: 185–188

Pankow J F. 1994b. An absorption model of the gas/aerosol partitioning involved in the formation of secondary organic aerosol. Atmos Environ, 28: 189–193

Smith D F, Kleindienst T E, McIver C D. 1999. Primary product distributions from the reaction of OH with *m*-, *p*-xylene, 1, 2, 4- and 1, 3, 5-trimethylbenzene. J Atmos Chem, 34: 339–364

Song C, Na K, Cocker III D R. 2005. Impact of the hydrocarbon to NO_x ratio on secondary organic aerosol formation. Environ Sci Technol, 39: 3143–3149

Takekawa H, Minoura H, Yamazaki S. 2003. Temperature dependence of secondary organic aerosol formation by photo-oxidation of hydrocarbons. Atmos Environ, 37: 3413–3424

Tong S R, Wu L Y, Ge M F, et al. 2010. Heterogeneous chemistry of monocarboxylic acids on α-Al_2O_3 at different relative humidities. Atmos Chem Phys, 10: 7561–7574

Usher C R, Michel A E, Grassian V H. 2003. Reactions on mineral dust. Chem Rev, 103: 4883–4940

Wang S, Wu D, Wang X M, et al. 2013. Relative contributions of secondary organic aerosol formation from toluene, xylenes, isoprene, and monoterpenes in Hong Kong and Guangzhou in the Pearl River Delta, China: An emission-based box modeling study. J Geophys Res, 118: 507–519

Warren D R, Seinfeld J H. 1985. Simulation of aerosol size distribution evolution in systems with simultaneous nucleation, condensation, and coagulation. Aerosol Sci Technol, 4: 31–43

White S J, Jamie I M, Angove D E. 2014. Chemical characterisation of semi-volatile and aerosol compounds from the photooxidation of toluene and NO_x. Atmos Environ, 83: 237–244

Wine P H, Nicovich J M. 2012. Atmospheric radical chemistry. In: Chatgilialoglu C, Studer A, eds. Encyclopedia of Radicals in Chemistry, Biology and Materials. New York: John Wiley & Sons, Ltd. 503–528

Zhang R, Xu Y, Han Z. 2004. A comparison analysis of chemical composition of aerosols in the dust and non-dust periods in beijing. Adv Atmos Sci, 21: 300–305

Zhang X Y, Sun J Y, Wang Y Q, et al. 2013. Factors contributing to haze and fog in China (in Chinese). Chin Sci Bull, 58: 1178–1187

Zhang X Y, Wang Y Q, Niu T, et al. 2012. Atmospheric aerosol compositions in China: Spatial/temporal variability, chemical signature, regional haze distribution and comparisons with global aerosols. Atmos Chem Phys, 12: 779–799

Zhang Y, Li C, Wang X, et al. 2012. Rush-hour aromatic and chlorinated hydrocarbons in selected subway stations of Shanghai, China. J Environ Sci, 24: 131–141

Zhang Y, Wang X, Barletta B, et al. 2013. Source attributions of hazardous aromatic hydrocarbons in urban, suburban and rural areas in the Pearl River Delta (PRD) region. J Hazard Mater, 250: 403–411

Zhao Z, Hao J M, Li J H, et al. 2008. Second organic aerosol formation by irradiation of α-pinene-NO_x-H_2O in an indoor smog chamber for atmospheric chemistry and physics. Chin Sci Bull, 53: 3294–3300

Zhou Y, Zhang H, Parikh H M, et al. 2011. Secondary organic aerosol formation from xylenes and mixtures of toluene and xylenes in an atmospheric urban hydrocarbon mixture: Water and particle seed effects (II). Atmos Environ, 45: 3882–3890